J. exp. Biol. 151, 219–244 (1990)
Printed in Great Britain © The Company of Biologists Limited 1990

LINEAR AND NONLINEAR ENCODING PROPERTIES OF AN IDENTIFIED MECHANORECEPTOR ON THE FLY WING MEASURED WITH MECHANICAL NOISE STIMULI

BY MICHAEL H. DICKINSON*

Department of Zoology NJ-15, University of Washington, Seattle, WA 98195, USA

Accepted 16 February 1990

Summary

The wing blades of most flies contain a small set of distal campaniform sensilla, mechanoreceptors that respond to deformations of the cuticle. This paper describes a method of analysis based upon mechanical noise stimuli which is used to quantify the encoding properties of one of these sensilla (the d-HCV cell) on the wing of the blowfly *Calliphora vomitoria* (L.). The neurone is modelled as two components, a linear filter that accounts for the frequency response and phase characteristics of the cell, followed by a static nonlinearity that limits the spike discharge to a narrow portion of the stimulus cycle. The model is successful in predicting the response of campaniform neurones to arbitrary stimuli, and provides a convenient method for quantifying the encoding properties of the sensilla.

The d-HCV neurone is only broadly frequency tuned, but its maximal response near 150 Hz corresponds to the wingbeat frequency of *Calliphora*. In the range of frequencies likely to be encountered during flight, the d-HCV neurone fires a single phase-locked action potential for each stimulus cycle. The phase lag of the cell decreases linearly with increasing frequency such that the absolute delay between stimulus and response remains nearly constant. Thus, during flight the neurone is capable of firing one precisely timed action potential during each wingbeat, and might be used to modulate motor activity that requires afferent input on a cycle-by-cycle basis.

Introduction

Unlike the rigid aerofoils of man-made flying machines, insect wings are flexible structures that bend during flight and other behaviour (Wooton, 1981). A recent theoretical analysis of flapping flight suggests that passive deformations may greatly augment wing performance by unsteady mechanisms (Daniel, 1987). Wing deformations have already been implicated in a number of aerodynamic mechan-

*Present address: Department of Neuroscience, Roche Institute of Molecular Biology, 340 Kingsland Street, Nutley, NJ 07110-1199, USA.

Key words: campaniform sensilla, white noise analysis, fly wings.

isms, such as increased lift due to camber (Vogel, 1967), the clap-and-fling (Weis-Fogh, 1973; Ellington, 1984*b*; Götz, 1986), vortex shedding (Nachtigall, 1981; Ellington, 1984*b*) and the maintenance of optimal angle of attack along the leading edge (Wooton, 1981; Ennos, 1988*a*). Whatever the actual role of wing deformations in force generation, it would appear that they are of some interest to the insect because wings are equipped with complex fields of campaniform sensilla (Zacwilichowski, 1931), mechanosensory structures innervated by single neurones (Moran *et al.* 1971), designed to detect strains in the exoskeleton (Spinola and Chapman, 1975). In locusts campaniform sensilla are capable of entraining the flight rhythm (Horsmann and Wendler, 1985) and appear to mediate corrective reflexes *via* connections with flight motor neurones and interneurones (Elson, 1978*a*,*b*,*c*). It is not known, however, what functions the wing campaniform neurones perform in the modulation of flight or other behaviour in flies. Since sensory neurones are commonly tuned for reception of behaviourally relevant stimuli, it should be possible to gain insight into the role of the campaniform sensilla on the fly wing by examining their encoding properties. This paper describes a method of analysis, using mechanical noise stimuli, designed to quantify the response characteristics of the campaniform neurones to stimuli relevant in flight behaviour.

Each fly wing contains approximately 70 campaniforms that may be divided into two groups based on their size and central projections. Over 60 small proximal campaniforms are found near the wing base organized in several discrete arrays (Cole and Palka, 1982; Gnatzy *et al.* 1987). In this location the sensilla should be most sensitive to deformations of the wing blade relative to the wing base or thorax. The axons from these small proximal campaniforms project to the dorsal portion of the thoracic ganglion (Ghysen, 1978; Palka *et al.* 1979) and these sensilla are probably responsible for the modulation of the head roll reflex by static wing loading (Hengstenberg, 1988). Ten larger campaniforms are more widely spaced from their neighbours and are not restricted to the wing base region. These sensilla are easily identified by their stereotypic positions on the wing (see Fig. 1A). As a consequence of their more distal position, many of these neurones can respond to intrinsic deformations of the wing blade. In *Drosophila*, nine of these cells segregate in either of two ventral tracts in the central nervous system (CNS) according to their physiological characteristics (Palka *et al.* 1986; Dickinson and Palka, 1987). Cells that adapt extremely rapidly to a constant deformation project to the medial tract, and neurones that adapt more slowly project together in the lateral tract. This dichotomy also correlates with birthdate, such that the four rapidly adapting cells of the medial tract are born several hours earlier (near the time of pupariation) than the four slowly adapting lateral tract neurones. The one exception to this chronological pattern is the dorsal humeral cross-vein sensillum (d-HCV), analyzed here, that is born early and follows the medial tract yet possesses the slowly adapting physiology. The subdivision of campaniform sensilla into discrete physiological and anatomical classes prompted the quantitative analysis contained in the present series of papers.

The campaniform neurone is modelled here as a Wiener cascade, a linear filter followed by a static (no memory) nonlinear encoder (see Fig. 3), two functions that can be easily measured in individual cells by recording the responses elicited by mechanical noise stimuli. This simple model serves several functions. First, it has predictive value; once the response of a sensory neurone has been characterized using the white noise approach, it is possible to predict the response to any arbitrary stimulus. Second, the model offers a useful set of functions for probing the processes of coupling, transduction and encoding in the campaniform sensilla. Third, the model provides a series of descriptive parameters that are unique for each neurone and therefore serve as a useful basis for comparisons among campaniform neurones or other mechanoreceptors. This paper describes the method of analysis in detail and presents results from experiments on the d-HCV sensillum on the wing of *Calliphora vomitoria*. In a companion paper (Dickinson, 1990), these methods are used to compare the physiological and mechanical properties among the other campaniform sensilla on the wing blade and to develop a model for the function of these mechanoreceptors in flight.

Materials and methods

Animals

All experiments were performed on 1- to 3-week-old blowflies, *Calliphora vomitoria*, purchased as third-instar larvae from College Biological Supply Co., Bothell, WA, USA. After emergence, the flies were housed in wire mesh cages, and maintained on a diet of sucrose, powdered milk and water.

Electrophysiology

The general recording techniques used in this study have been described previously (Dickinson and Palka, 1987). However, several modifications were necessary to allow for more precise stimulation of the campaniform sensilla and measurement of mechanical properties (Fig. 1B,C). Following anaesthetization of a fly in CO_2, a wing was excised leaving a small piece of thoracic cuticle attached. The wing was fixed with cyanoacrylate to the surface of a glass coverslip mounted rigidly to the top of a 6 mm thick acrylic block. Before gluing the wing to the stage, the surface of the glass coverslip was lightly coated with Zip Kicker (Pacer), which sets cyanoacrylate instantly and allows the adhesive to harden across large gaps, such as those produced by the corrugations of the wing. The gluing agents had no adverse effects upon the responses of the sensory neurones compared to wings mounted using petroleum jelly. The proximal and distal ends of the wing made fluid contact with insect saline contained in small wells milled into the acrylic chamber. The two wells contained silver electrodes that connected to a differential amplifier with a 500 MΩ input impedance. A window discriminator was used on line to transform each action potential into a 200-μs square pulse.

This differential extracellular technique apparently records the action potentials at the site of spike initiation *via* the resistive pathways provided by the wings veins.

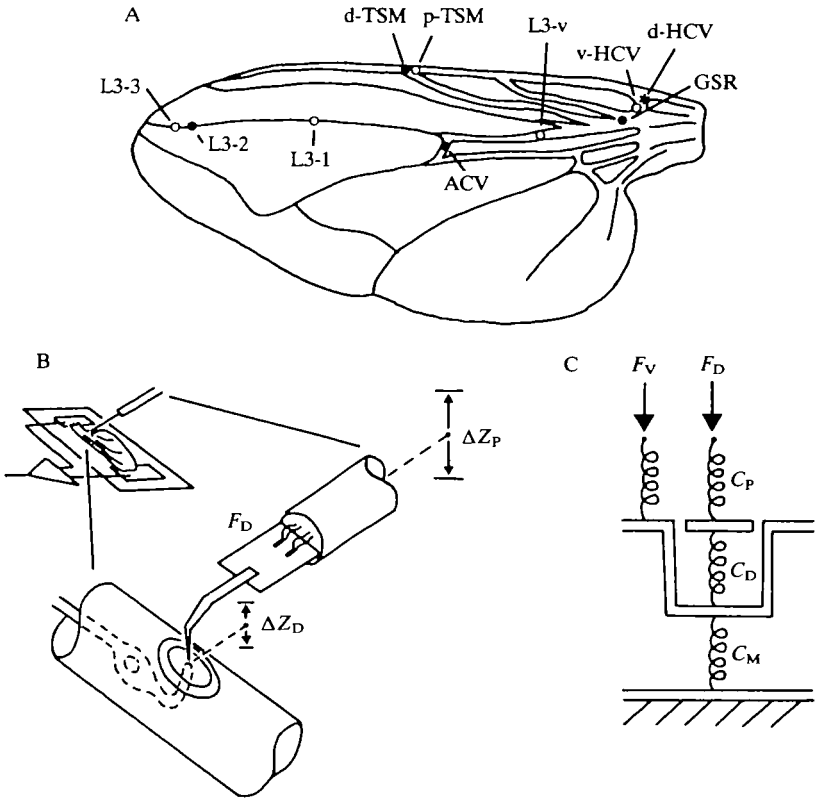

Fig. 1. Schematic drawings illustrating experimental methods. (A) Diagram of *Calliphora* wing showing position of large distal campaniform sensilla. The *Calliphora* wing is approximately 8 mm in length. Neurones whose axons travel in the medial and lateral tracts in the CNS, based on homologous cells in *Drosophila*, are indicated with closed and open circles, respectively. d-HCV and v-HCV, dorsal and ventral humeral cross-vein sensilla: GSR, giant sensillum of the radius; p-TSM and d-TSM, proximal and distal twin sensilla of the margin; L3-v, ventral sensillum of the third vein: L3-1, L3-2, L3-3, first, second and third sensilla of the third vein; ACV, anterior cross-vein sensillum. All the campaniform sensilla are on the dorsal surface of the wing except for v-HCV and L3-v. The encoding properties of the d-HCV neurone are analysed in this paper. (B) Stimulation and recording methods. Both ends of the rigidly fixed wing make contact with saline wells containing the extracellular electrodes (inset). The etched tungsten tip, in series with a force gauge, is brought to rest on the surface of the campaniform dome. The displacement of the proximal end of the probe, ΔZ_P, is measured directly with a displacement transducer. The much smaller displacement of the campaniform dome, ΔZ_D, is calculated using the compliance model indicated schematically in C. (C) The probe, preparation and mounting chamber are modelled as a series of three elastic elements (see Materials and methods). Force-indentation measurements are made with the probe either directly on the campaniform dome (F_D) or on an adjacent vein cuticle (F_V), and the compliance due to the campaniform sensillum is found by subtraction. The indentation of the campaniform dome is then calculated as the product of force and compliance ($F_D C_D$). C_P and C_M are defined in the text.

This interpretation was based upon measurements of response latencies before and after shortening the conduction path by cutting the proximal portion of the wing. Individual campaniform sensilla were stimulated with short trapezoidal deformations that elicited single action potentials. The proximal portion of the wing containing the axon was then cut and the stimuli repeated. Shortening the axon length had no effect on the response latencies to the indentations, or on the shapes of $g(t)$ functions measured using noise stimuli (see below). Thus, there is no delay prior to the initial rise of the extracellular signal that might be due to the propagation of the action potential down the axon. The size of the extracellular spikes was often increased after shortening the wing, which would be expected if the wing veins act as resistive pathways to the spike initiation site.

Mechanical stimulation

The method of direct punctate indentation used in the present study is adapted from the techniques developed for cockroach campaniform sensilla, where proprioception is known to be mediated by a 10–100 nm indentation of the cuticular dome (Chapman *et al.* 1973; Spinola and Chapman, 1975; Chapman and Duckrow, 1979). Mechanical deformations of the campaniform dome were produced by a stimulus probe mounted on a Ling model 201 vibration generator. Displacements of the vibration generator were monitored by two vertically aligned infrared transistors illuminated by a pair of light-emitting diodes. The light path between the emitters and detectors was interrupted by a stainless-steel flag mounted on the shaft of the vibration generator. At rest the flag was aligned so that it obscured the upper half of the lower detector and the lower half of the upper detector. The signals from the two phototransistors were amplified differentially and used with a proportional integrator–differentiator (PID) feedback circuit to control the output of the vibration generator. The stimulus signal used in these experiments was produced by a General Radio model 1390-B noise generator. It was recorded on magnetic tape and played back to the PID circuit at one-quarter speed through a low-pass 24 dB octave^{-1} Butterworth filter (Krohn-Hite model 3750) with a 3 dB setting at 500 Hz. *Calliphora* wingbeat frequency is approximately 150 Hz, and preliminary experiments indicated that the response of the d-HCV neurone fell substantially above 200 Hz. Therefore, the playback speed and filter settings were chosen to produce a flat response in the 20–400 Hz frequency range, which would include frequencies that the campaniforms are likely to encounter during flight.

The stimulus probe consisted of an electrolytically etched tungsten needle attached to a force transducer. The force transducer was constructed of four semiconductor strain gauges and mounted on 0.25 mm stainless-steel shim wired in a full-bridge configuration. The resonant frequency of the transducer was approximately 1 kHz. The tip of the tungsten probe contained two 45° bends arranged so that the distal 0.5 mm was aligned vertically. The end of the probe tapered to a parabolic tip, approximately 1 μm in diameter. The vibration generator with attached probe was mounted on a vertical micromanipulator which

was fixed to a translation stage allowing two axes of finely controlled horizontal motion.

Calibration

During experiments, the peak excursions of the vibration generator were approximately 1 μm. The output of the displacement transducer, calibrated with an eyepiece micrometer, was linear within this range with a slope of 0.24 μm V^{-1}. The force transducer was calibrated from the static loading of aluminium foil weights. The relationship between force and voltage was linear with a slope of 525 μN V^{-1}.

Data analysis

Fig. 2 shows an example of the raw data used in these experiments, photographed directly from the oscilloscope screen. The lowest trace is the position of the stimulus probe recorded at the shaft of the vibration generator during application of a noise stimulus. Immediately above is the force record. These two waveforms were used to calculate the mechanical compliance (indentation per unit force) of the campaniform dome. The top two traces show the spike train response of the d-HCV neurone and the pulse representation of the spike train.

Each set of experiments on an identified campaniform sensillum consisted of the following protocol. The stimulus probe was positioned over the d-HCV campaniform dome under visual control at 600× magnification. The vertical position of the stimulus probe was adjusted until a small 1–3 μN deflection was detected by the

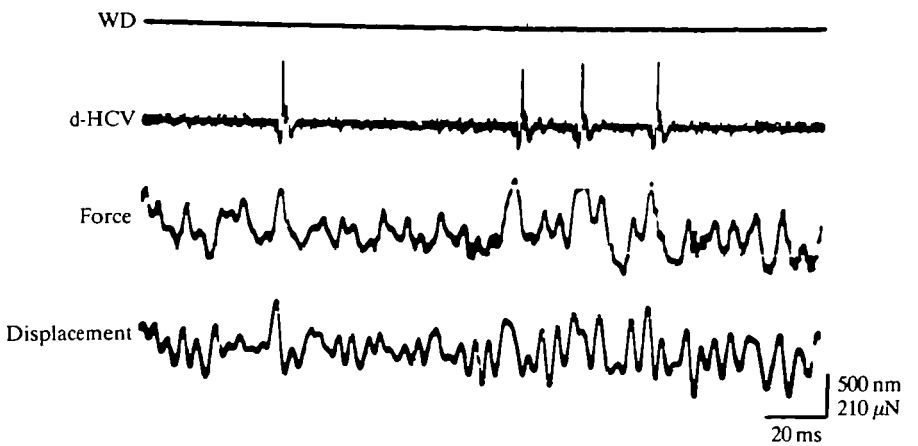

Fig. 2. Oscillogram showing sample raw data. The lower two traces show the displacement of the probe shaft and the output of the force gauge during a noise stimulus. The upper two traces show the raw spike train and its digital representation obtained using a window discriminator (WD). The force, displacement and digital spike train were sampled on-line by a computer at 5 kHz per channel and stored for subsequent analysis.

force transducer, indicating that the tungsten needle had made contact with the surface of the campaniform, yet exerted a negligible indentation force. The outputs of the force and displacement transducers were then adjusted to zero. Thus, stimulus force and probe displacement were always measured relative to the unloaded campaniform dome. The offset of the stimulus signal was then adjusted to produce a net indentation force of 10–100 μN. While monitoring the spike rate of the neurone, either by the output of a digital counter or through an audio monitor, a continuous noise stimulus was delivered to the cell, and the stimulus level was adjusted until a nearly maximal response was obtained. The magnitude of the stimulus offset was readjusted so that the probe was in contact with the campaniform dome throughout the stimulus. Once the stimulus magnitude and offset levels had been determined, a continuous noise stimulus was applied and, after waiting a few seconds for transient responses to decay, 5 s of data was recorded. These stimulus–response data were used to calculate the linear function $g(t)$. The campaniform neurone was subsequently stimulated using a shorter noise segment repeated 25 times, from which a 1 s section was averaged and used to construct the nonlinear function $m(\cdot)$. In most experiments a second short noise segment was applied repetitively and the response used to test the predictions of the Wiener cascade model.

After the last repetition of the stimulus, the stimulus probe was moved laterally to a point approximately 1–2 campaniform diameters away from the sensillum dome. Following readjustment of the force and displacement offsets, 1 s stimuli were applied at four equally spaced points in a circle around the sensillum. These measurements were required to determine the compliance of the wing vein. It was necessary to compute the average of four measurements, because the mechanical properties of the vein were found to vary spatially. The mean level and peak-to-peak displacements of these stimuli were identical to the values used for the stimulus applied directly to the campaniform dome.

The outputs of the displacement transducer and force probe and the digital representation of the spike train were sampled at 5 kHz per channel using a Zenith Z-200 PC series computer equipped with a Data Translation 2821 A/D converter and stored on computer diskettes for subsequent analysis.

Compliance computations

The force and displacement records were used to calculate the actual indentation of the campaniform dome by a method similar to that of Chapman and Duckrow (1975). Compliance may be defined as the vertical deformation per unit force applied at a single point. The stimulus probe, campaniform dome, wing vein and recording chamber are treated as a series of simple elastic components whose compliances sum (see Fig. 1C):

$$C_T = C_M + C_D + C_P . \tag{1}$$

The desired quantity C_D, the point compliance of the campaniform dome, may be calculated by subtraction from the total compliance, C_T, if the sum of the other

compliances is known. C_P accounts for all uninteresting sources of compliance between the displacement transducer and the tip of the tungsten needle. C_M includes all sources of compliance distal to the sensillum dome, such as the wing vein, the cyanoacrylate adhesive and the recording chamber. The sum of these two compliances may be calculated as follows:

$$C_M + C_P = \Delta Z_V / \Delta F_V , \tag{2}$$

where F_V is the force measured when the probe is placed on the vein cuticle adjacent to the campaniform, and Z_V is the vertical displacement measured at the vibration generator shaft. In practice, these compliances were calculated from the average of the four measurements made at equally spaced points around the campaniform dome. Because the dome compliance potentially influences the dynamic behaviour of the neurone, computations were made in the frequency domain:

$$C_D(f) = \frac{D(f)F(f)^*}{F(f)F(f)^*} , \tag{3}$$

where $F(f)$ and $D(f)$ are the Fourier transformations of the force and displacement records from a noise stimulus experiment, and an asterisk denotes a complex conjugate. Once the compliance of an individual campaniform dome had been determined, the actual dome indentation in each experiment was calculated by multiplying C_D by the indentation force.

Systems analysis

Through the use of a Gaussian white noise stimulus, any dynamic system may be characterized as a Wiener functional expansion, consisting of a series of convolution integrals (Marmarelis and Marmarelis, 1978). Each term in the series is an nth-order convolution of the input with the nth-order kernel of the system. The first-order kernel of the series accounts for the linear behaviour of the system and is loosely analogous with the transfer function of a linear system. For a neurone that fires action potentials in response to a stimulus, the first-order kernel may be defined as (see Appendix):

$$h_1(t) = \xi x_i(t) , \tag{4}$$

where $x_i(t)$ is the signal average of the stimulus record preceding the occurrence of each action potential when the cell is driven using a noise input (see Bryant and Segundo, 1976, for a similar derivation). Thus, the $x_i(t)$ function represents the average stimulus segment most likely to produce an action potential in the sensory neurone, and acts as a 'template' that may be used to compare the response properties of different cells. The scalar ξ is a sensitivity parameter defined as the mean spike rate divided by the power level of the stimulus. Because a band-limited noise input is used, the power level is estimated as the area under the autocorrelation function of the stimulus (Marmarelis and Marmarelis, 1978). Thus, the quantity ξ has units $(\text{spikes}\,\text{s}^{-1})(\text{nm}^2\,\text{s})^{-1}$. If the mean firing rate of the

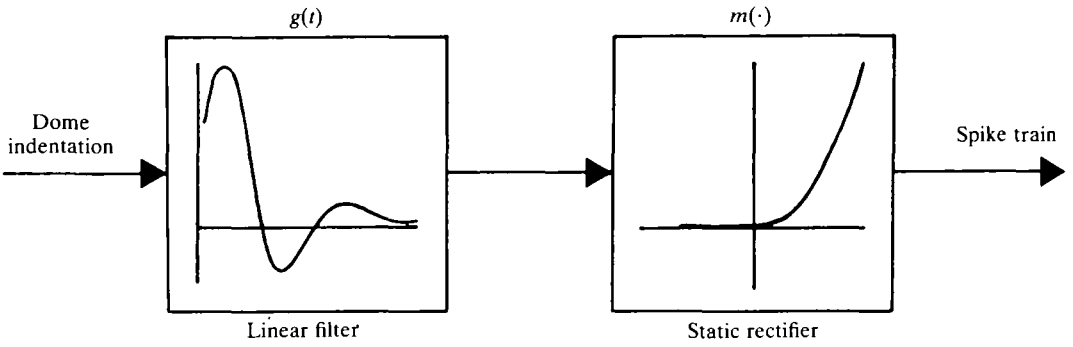

Fig. 3. Wiener cascade model of campaniform encoding. According to this proposed model, a linear filter, $g(t)$ and a static nonlinearity, $m(\cdot)$ are arranged in series, linking dome indentation and the spike train of the mechanosensory neurone. The linear element first filters the stimulus, accounting for the gross characteristics of the frequency sensitivity of the neurone and its phase characteristics. The output of the filter is subsequently rectified, limiting the final spike discharge to only a portion of a stimulus cycle.

neurone is high or the power level of the stimulus is low, then the sensitivity of the neurone is large. Once the function $h_1(t)$ has been calculated, it may be convolved with any arbitrary stimulus waveform to construct a linear prediction of a neurone's response (see Appendix).

A dynamic system that is composed of a linear filter followed by a static (no memory) nonlinearity is called a Wiener system (this established nomenclature is awkward, and the Wiener system should not be confused with 'Wiener system analysis' employing the Wiener series expansion of equation A1. To avoid confusion, I will use the term 'Wiener cascade' to describe the simple cascade shown in Fig. 3). Following the nomenclature of Hunter and Korenberg (1986), the linear and nonlinear components of a Wiener cascade are termed, respectively, $g(t)$ and $m(\cdot)$. The time domain relationships between $g(t)$ and the first- and second-order Wiener series kernels of the system are (Marmarelis and Naka, 1972; Marmarelis and Marmarelis, 1978):

$$h_1(t) = C_1 g(t)\,, \tag{5}$$

$$h_2(t_1,t_2) = C_2 g(t_1) g(t_2)\,, \tag{6}$$

where C_1 and C_2 constants. Thus, the first component of an unknown Wiener cascade is found by measuring the first-order kernel of the Wiener series. In addition, equation 6 offers a convenient means of testing the validity of the Wiener cascade model. The first-order kernel $h_1(t)$ is measured, and the shape of the second-order kernel $h_2(t_1,t_2)$ is calculated. This may then be compared to an experimental estimate of the second-order kernel.

The static nonlinear function, $m(\cdot)$, may be constructed by stimulating the neurone with a noise stimulus and plotting the average response against the prediction of the linear model. The averaging process introduces artificially high

frequency components in the response data that are smoothed using an appropriate digital filter. The resulting spread of data points is then fitted to a polynomial function that defines $m(\cdot)$. Any nonlinear behaviour, such as rectification, is clearly seen as a deviation from a 1:1 relationship between the measured response and the linear prediction. Once $m(\cdot)$ has been estimated it may be coupled with $g(t)$ to produce the full nonlinear model of Fig. 3. This experimentally estimated Wiener cascade model can then be used to predict the response to any arbitrary stimulus.

Results

Compliance and sensitivity

The compliance of the d-HCV campaniform, as measured by punctate stimulation, was relatively constant throughout the frequency range 125 Hz above and below wingbeat frequency. Fig. 4A shows a sample calculation of dome compliance by subtraction of extraneous compliances contributed by stimulus, probe, vein and wing adhesive. The values of compliance as a function of frequency were calculated through transformations and computations in the frequency domain, as described in the Materials and methods section. Typically, the ratio of total compliance to dome compliance (C_T/C_D) was 10 to 1.

The resultant regressions fitted to dome compliance are indicated in Fig. 4B for 12 preparations. The 95% confidence interval for the regression coefficient included the zero slope value in all preparations (Sokal and Rohlf, 1981), indicating that the campaniform domes exhibit purely elastic behaviour within the range of loading frequencies surrounding wingbeat frequency. Because the compliances do not depend significantly upon frequency, the value at 150 Hz (C_{150}) was chosen as a standard for comparisons of compliance and in the calculations of displacement from the force records. The C_{150} values for each preparation are given in Table 1. The mean value of C_{150} was 0.66 ± 0.24 nm μN^{-1} (S.D., $N=11$), which is consistent with the dome compliance reported for tibial campaniform sensilla of the cockroach (Chapman and Duckrow, 1975).

Because the goal of these experiments was to quantify the behaviourally relevant encoding properties of a sensory neurone, it was crucial to choose an appropriate stimulus level. In the absence of any direct knowledge about the stimulus magnitudes encountered during flight, the following paradigm for setting the stimulus magnitude, based on preliminary measurements of campaniform sensitivity for several d-HCV neurones, was adopted. The mean spike rate plotted against stimulus power for four individual neurones is shown in Fig. 5. The stimulus–response relationship is approximated by the equation: $y=57.6+53.6\log x$, found by least-squares regression through the pooled data points. The spike rate increases very gradually for stimulus levels above 4 nm^2 s. In all subsequent experiments, the stimulus power levels were set to produce a near maximal response (see Materials and methods). These values are listed in Table 1. The mean power level for all experiments was 6.85 ± 4.43 nm^2 s (S.D., $N=11$). The

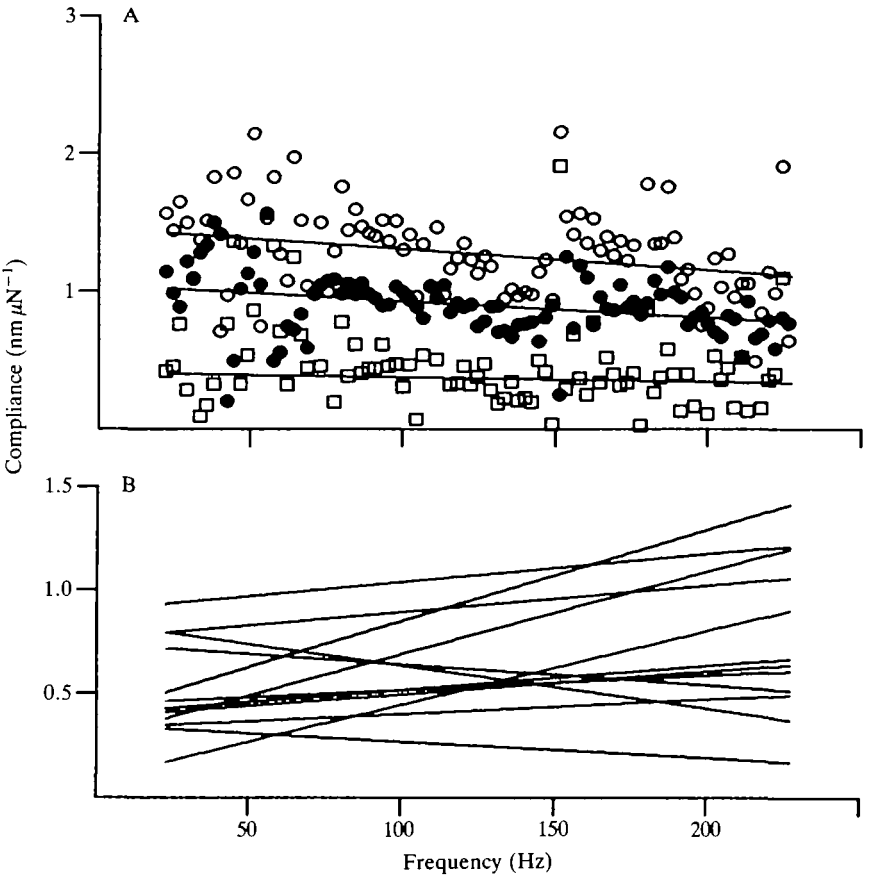

Fig. 4. Compliance measurements of d-HCV sensilla. (A) A sample calculation of the dome compliance (cell 3) by subtraction of series elements. The compliances were computed in the frequency domain from 25 to 275 Hz. The open circles show the total compliance calculated with the force probe positioned on the campaniform dome. The closed circles show the average of four compliance measurements made in a circle around the sensillum. The difference between these two measurements, the dome compliance, is indicated by open squares. The solid lines represent least-squares regressions through the three data sets. (B) A set of regressions through the campaniform compliance measurements for 12 separate preparations. There is no consistent trend in the rate sensitivity of the campaniform compliance among the 12 sensilla, and the slope value of 0 fell within the 95% confidence intervals of the regression in all cases (Sokal and Rohlf, 1981).

ratio of mean spike rate to stimulus power is the sensitivity parameter ξ, which is listed in Table 1 and used in calculations of the linear function $g(t)$.

Linear filter and static rectifier functions

Fig. 6 illustrates calculations of $g(t)$ and $m(\cdot)$, the dynamic linear and the static nonlinear functions of the Wiener cascade model. The superposition of 50 stimulus

Table 1. *Compliance, mean spike rate, stimulus power and sensitivity (ξ), measured for individual d-HCV neurones*

Cell	Compliance (nm μN^{-1})	Spike rate (spikes s^{-1})	Power (nm^2 s)	ξ (spikes s^{-1})(nm^2 s)$^{-1}$
1	0.57	163.8	6.70	24.5
2	0.54	135.7	4.15	26.4
3	0.56	144.8	4.04	35.8
4	0.43	86.5	3.39	25.5
5	0.94	91.3	10.98	8.3
6	0.54	120.4	4.85	24.8
7	0.61	88.9	3.64	24.5
8	0.83	95.0	9.07	10.5
9	0.56	96.2	4.94	19.5
10	0.24	111.3	1.46	76.2
11	1.09	97.8	18.52	5.3
Mean (N=11)	0.66	116.9	6.85	24.9
S.D.	0.24	28.7	4.43	17.6

Compliance was measured at a loading frequency of 150 Hz.

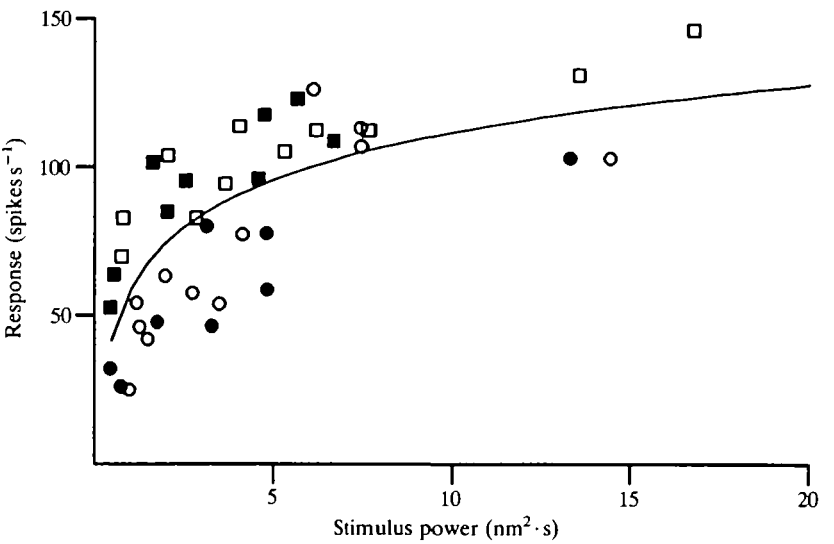

Fig. 5. Sensitivity of the d-HCV neurone to stimulus power level. The mean spike level during a 5 s mechanical noise stimulus is plotted against the power level for four preparations, each represented by a different symbol. The spike rate at the lowest stimulus levels reflects the sensitivity to steady-state deformation that is present in these slowly adapting mechanoreceptors. The response rises with increasing power level and reaches a near maximal value at a power level of 6 nm^2 s. The relationship is approximated by the equation: $y=57.6+53.6 \log x$ (solid line), found by least-squares regression through the data points pooled from all four preparations.

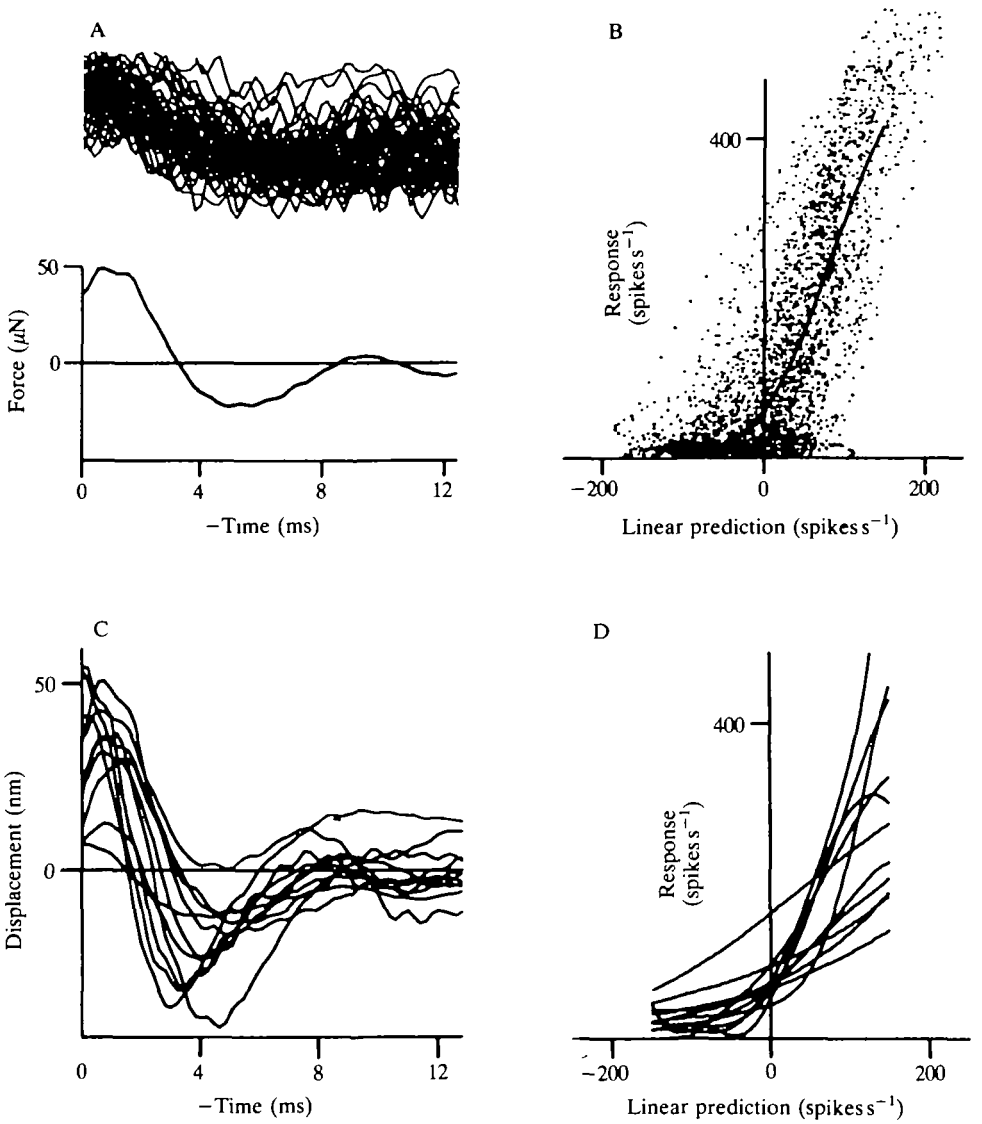

Fig. 6. Calculation of dynamic filter and static nonlinear functions. (A) Top panel shows the superposition of 50 stimulus traces preceding spike occurrences during noise stimulation. The time axis is reversed such that time preceding spike occurrence is plotted from left to right. The bottom panel shows the stimulus average over the entire record (602 spikes) for a campaniform neurone (cell 6). The individual traces are shown at half the gain of the average trace. (B) The function in A was used to construct a linear prediction of the cell to a novel noise stimulus. The linear model is plotted point for point against the actual averaged response. The static nonlinear function is constructed by the least-squares fit of a sixth- order polynomial through the spread of points. The first-order functions, $g(t)$, and static nonlinearities, $m(\cdot)$, measured from 11 separate preparations are shown in C and D, respectively.

waveforms preceding the occurrence of spikes in the d-HCV neurone is shown in the upper part of Fig. 6A (cell 6). The average over the entire 5 s stimulus (602 spikes) is shown below. The value of ξ, the sensitivity parameter, for this neurone was 24.8 (spikes s^{-1})(nm^2 s)$^{-1}$. The $g(t)$ function in Fig. 6A was used to predict the linear response of the neurone to a repetitive stimulus (see Fig. 7). In Fig. 6B, this prediction is plotted against the measured average response. The resultant spread of points is then fitted with a sixth-order polynomial to yield the static nonlinear function $m(\cdot)$. Fig. 6C,D shows the variability of these functions calculated for all 11 preparations.

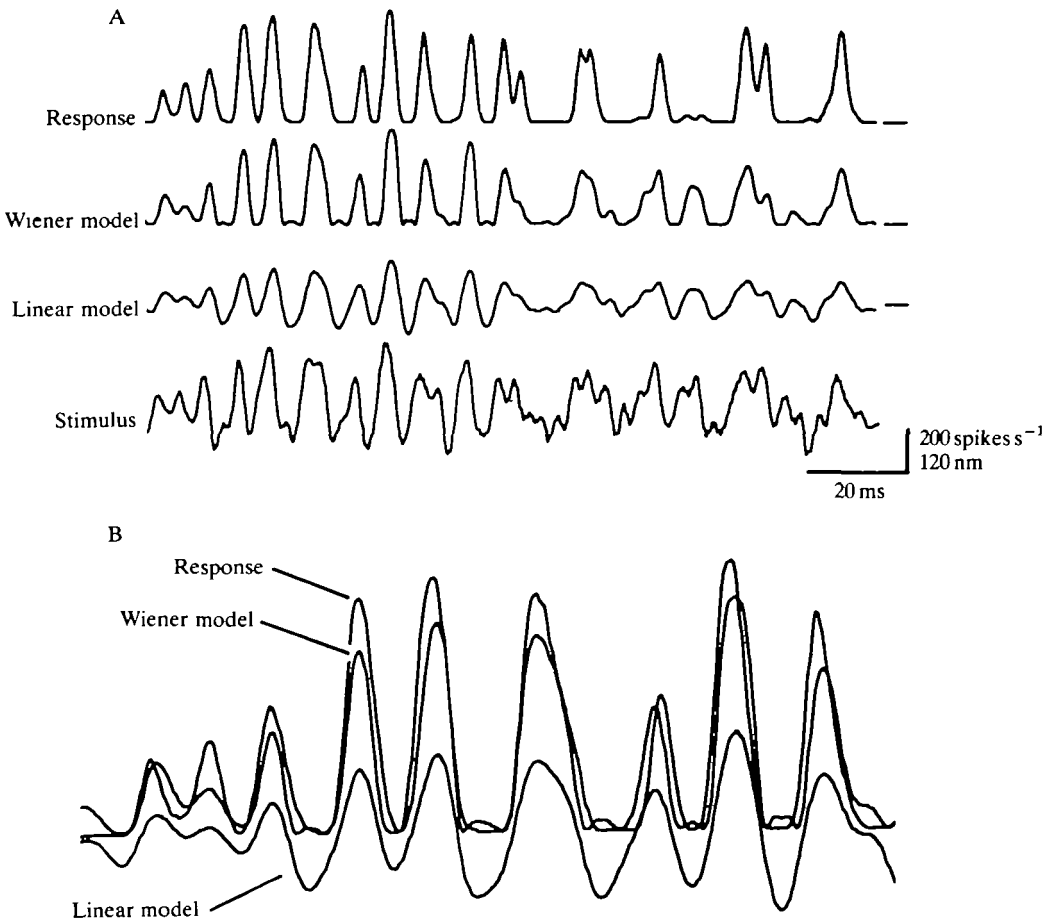

Fig. 7. Predictions of the Wiener cascade model. The averaged spike frequency in response to a noise stimulus is compared to the prediction of the full Wiener cascade model and that of the linear term alone (cell 6). (A) The top trace shows the measured response averaged over 25 repetitions. The Wiener cascade model, constructed with both the linear and the nonlinear functions shown in Fig. 6, is substantially more accurate in describing the behaviour of this neurone than the simple linear model. The lower trace shows the average noise stimulus. (B) Superposition of the measured response and model predictions at higher resolution (2× gain and 3× time base).

Fig. 7 demonstrates the predictive strength of the Wiener model. The functions shown in Fig. 6A,B were used to calculate the predictions for the noise segment indicated in Fig. 7A. The linear model, Wiener cascade model and measured response are superimposed on an expanded time scale in Fig. 7B. The linear model alone does not yield an accurate prediction. The $m(\cdot)$ function amplifies and rectifies the linear prediction, and the resultant full Wiener cascade model is more accurate in predicting the average response of the neurone to the repetitive stimulus. The performance of the model may be quantified by calculating the mean square error (MSE) between the predictions and the measured response, normalized to the MSE computed for the mean response level (Marmarelis and Marmarelis, 1978). The MSEs for the linear model and the Wiener cascade model shown in Fig. 6 are 108% and 26%, respectively. Thus, the addition of the nonlinear element greatly improves the predictive performance of the model.

A threshold criterion may be added to the output of the Wiener model to predict spike occurrence times (Korenberg *et al.* 1988). In the simplest scheme, the model produces an action potential at the peak value of any excursion of the predicted waveform above some arbitrary threshold. Such a calculation is shown in Fig. 8 (cell 3). A prediction was calculated for a short segment of noise and compared to the actual spike discharge of the neurone. The threshold level was arbitrarily changed until the spike pattern of the model most closely resembled that of the actual sensory cell. There are some discrepancies in the timing of firing, but the fit is quite good. Thus, the model can in large part account for the firing patterns resulting from a single noise stimulus.

The first- and second-order kernels $[h_1(t),h_2(t_1,t_2)]$ of the Wiener series functional expansion of any Wiener cascade are related in a calculable manner (Marmarelis and Marmarelis, 1978). Thus, the appropriateness of the Wiener cascade model may be tested by measuring directly the second-order kernel from the preparation and comparing it to the kernel computed for a true Wiener cascade. As shown in Fig. 9, there is a close resemblance, indicating that the Wiener cascade model is a reasonable predictor of complex dynamic behaviour of the neurone.

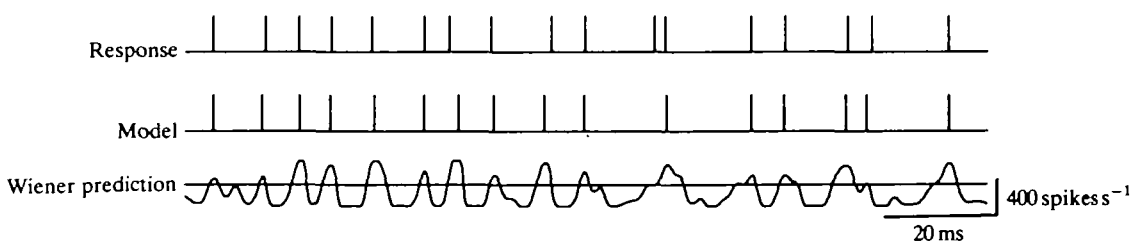

Fig. 8. The spike discharge produced by a single stimulus is compared to the predictions of the Wiener cascade model (cell 3). The bottom trace shows the response predicted by the model for a noise stimulus. The model 'fires' a spike at the peak of any excursion of the continuous model above an arbitrary threshold level, set to produce the closest match by eye to the actual response, shown in the top trace.

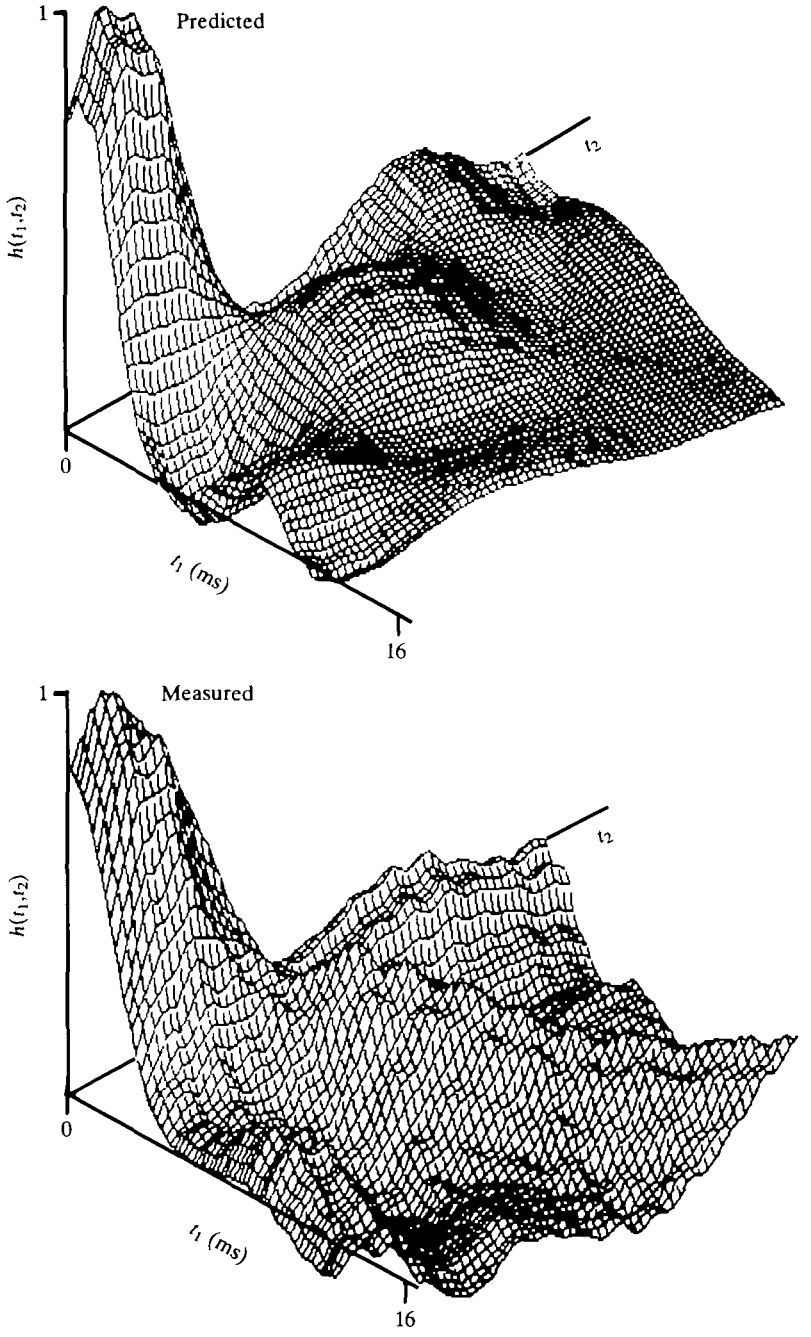

Fig. 9

Frequency response and sensitivity

Fourier transformation of the characteristic function $g(t)$ provides a convenient method for estimating the nonlinear transfer function representing the sensitivity of the campaniform neurones (Marmarelis, 1988). The frequency responses

Fig. 9. Comparison of predicted and calculated second-order kernels. The second-order kernel in the top panel was computed assuming that the neurone is structured as a Wiener cascade, with a linear filter followed in series by a static nonlinearity. The bottom panel shows the second-order kernel calculated from an experimental record (cell 6). The kernels have units of spikes s^{-1} nm^{-2} s^{-2}, but both functions have been normalized to facilitate comparison of their shapes. If the nonlinearity preceded the linear filter, the second-order kernel should be zero everywhere except along the diagonal where $t_1=t_2$.

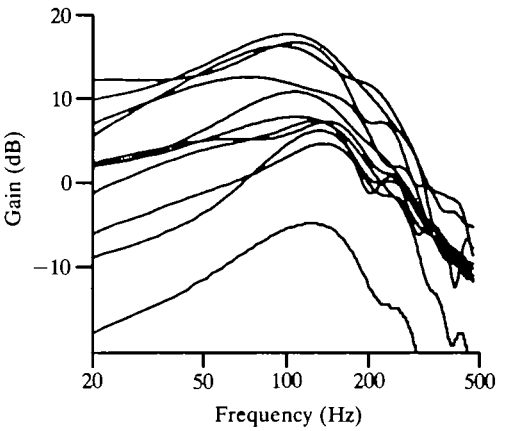

Fig. 10. The system transfer functions for the d-HCV neurones calculated from the functions of Fig. 6C (N=11). The gain in spikes s^{-1} nm^{-1} is plotted on a decibel scale. All the neurones possessed a broad response peak near 150 Hz, corresponding to the wingbeat frequency of *Calliphora*, and a cut-off frequency below 200 Hz.

calculated from the data of Fig. 6C are indicated in Fig. 10. Individual neurones differ somewhat in the exact level of sensitivity, but all the cells show a broad sensitivity peak at 150 Hz, which corresponds to the wingbeat frequency of *Calliphora*. The decay in response above 150 Hz is approximately 10 dB octave^{-1}.

Phase characteristics

If the campaniform sensory neurone acts as a true Wiener cascade, the phase response of the neurone should be established entirely by the linear filter, because the nonlinearity is a static function. Fig. 11A shows the results of an experiment in which a neurone (cell 3) was stimulated with 25 repetitions of a 1-s sine wave sweep encompassing one order of magnitude from 25 to 250 Hz. Above 40 Hz the averaged response of the neurone to each cycle of stimulation was smooth and unimodal, indicating that the cell responds to each oscillation with a single action potential. The response leads the stimulus at low frequencies, crosses zero near 80 Hz, and lags at high frequencies. In the range of frequencies surrounding wingbeat frequency, the delay between stimulus and response is a nearly constant value of 0.7 ms. The solid line in Fig. 11B was constructed from Fourier

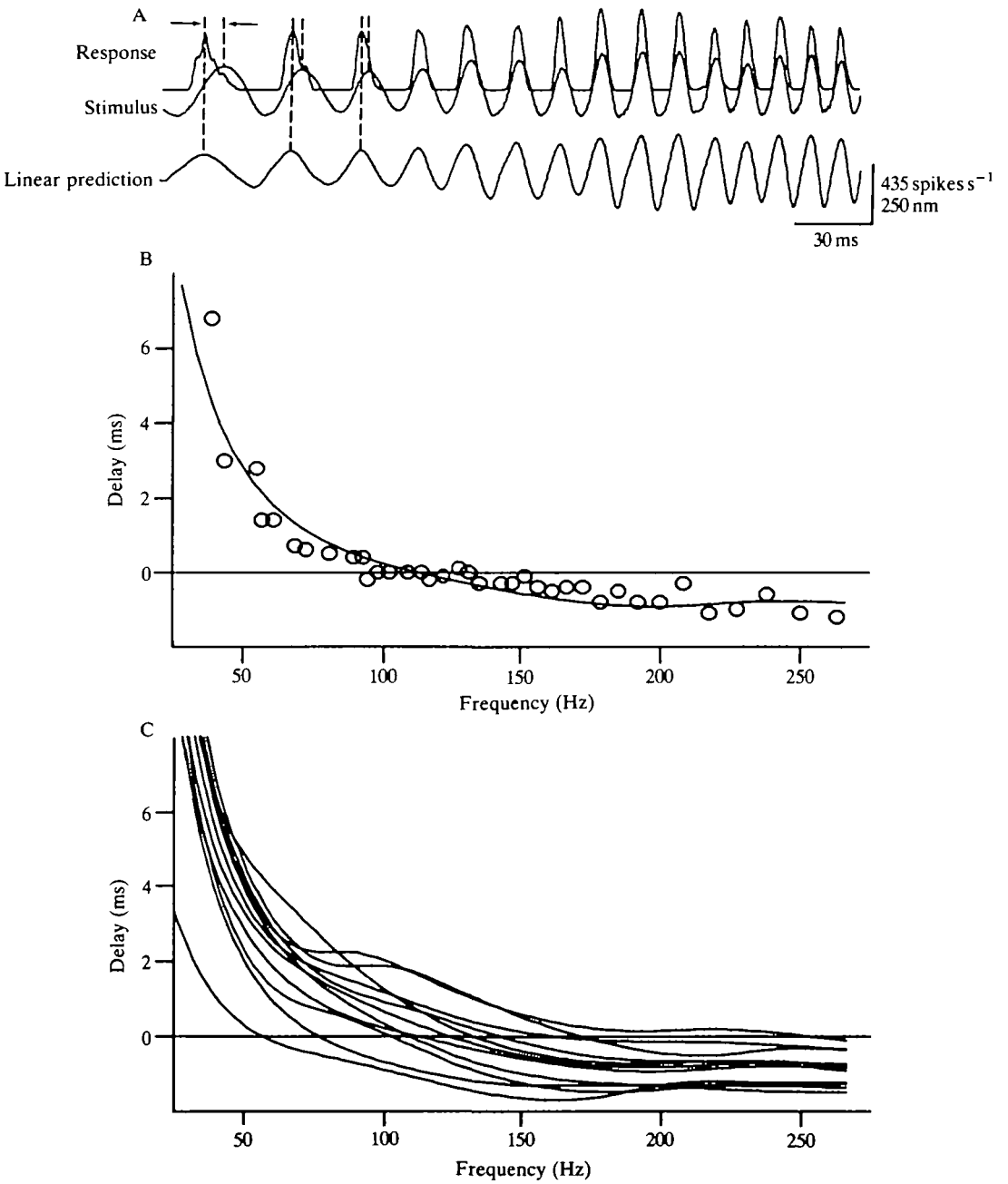

Fig. 11

transformation of the $g(t)$ function measured for this neurone. The complex behaviour of the measured delay is accurately predicted by the linear element. The phase predictions generated from the Fourier transformations of the $g(t)$ functions in Fig. 6C are consistent among individual d-HCV neurones, as shown in Fig. 11C.

In summary, the Wiener cascade model is a reasonably accurate predictor of the

Fig. 11. Phase relationships between stimulus and response. (A) The upper two superimposed traces show the response of a campaniform neurone to a sinusoidal stimulus of linearly increasing frequency, averaged over 25 repetitions. At lower frequencies the response leads the stimulus. The lower trace is a prediction of the linear model. The linear model accurately predicts the phase relationship of the campaniform neurone (cell 3). (B) The measured and predicted phase relationship between stimulus and response are plotted in terms of the absolute time delay. The open circles are the measured peak-to-peak delays between stimulus and spike frequency response during the sinusoidal sweep shown in A. The smooth curve was generated from the Fourier transformation of the measured linear element $g(t)$ (Fig. 6). (C) Predicted delay functions for d-HCV neurones. The delay functions were computed from the Fourier transformation of the $g(t)$ functions in Fig. 6C. The delay between stimulus and response is relatively constant throughout the range of frequencies typical of wingbeat in *Calliphora*.

response behaviour of an identified campaniform sensory neurone. Therefore, the two functions of the model, the linear filter $g(t)$ and the static nonlinearity $m(\cdot)$, may be used as tools for comparing the response properties among other campaniform neurones or mechanoreceptors from different modalities.

Discussion

Function of d-HCV as an event detector

Although the gross wing kinematics of many dipteran species have been extensively quantified (Nachtigall, 1966; Vogel, 1967; Ellington, 1984*a*; Ennos, 1989), the fine details, such as the temporal and spatial patterns of deformations on the wing surface, have not yet been accurately determined (for a review of qualitative descriptions of wing deformations in flight, see Wooton, 1981). This, together with the complexity of wing architecture, makes it difficult to reconstruct the time course of strains that the d-HCV or any campaniform sensillum is likely to encounter during flight. Recently, Ennos (1988*a*,*b*) has examined the architecture of the dipteran wing with special emphasis on the passive deformations that result from torsion of the wing about the leading edge. He found that the wing architecture predicts that a distal–proximal torsional wave should travel along the wing, initiated during the rapid wing rotation that occurs at the beginning of each half-stroke. This torsional wave has been observed in ciné films of many large flies, and is particularly prominent during supination (Nachtigall, 1979; Wooton, 1981; Ellington, 1984*a*; Ennos, 1988*b*, 1989). Since the gross characteristics of this wave are produced by the rotation of the wing during each stroke, the dominant spectral component of wing torsion sensed by the campaniform neurones is probably at the natural wingbeat frequency. It is most likely that the d-HCV fires only a single action potential during each wingstroke, because the frequency response of the cell falls sharply at frequencies over 200 Hz (Fig. 10). The other campaniform neurones may also display this constraint, a hypothesis that is supported by the results of Heide (1983), who recorded the afferent activity from the wing nerve

during tethered flight in *Calliphora*. Although it is difficult to identify individual units in his compound recordings, it would appear that the wingbeat synchronous afferents fire single action potentials during each wingbeat. Based on axon diameter, the largest afferent spikes in wing nerve recordings are likely to be those of the distal campaniform neurones.

Thus, during flight the d-HCV probably fires one phase-locked action potential per wingbeat cycle. As shown in Fig. 11, the phase relationship between the stimulus and response is such that the absolute interval varies little throughout the range of wingbeat frequencies typical of *Calliphora*. Within this same range of frequencies, the d-HCV neurone exhibits little frequency sensitivity. Therefore, the cell appears well designed as a 'one-shot' event detector, responding to the deformational pattern produced during each wingbeat with a single action potential, at a fixed delay relative to the peak indentation of the dome. As argued more fully in the second paper of this series (Dickinson, 1990), an array of such sensors distributed along the wing might be used to monitor the movement of the distal–proximal torsional wave initiated during supination in each wingbeat.

Comparison of d-HCV with cockroach campaniform sensilla

It is useful to compare the encoding properties of the d-HCV neurone with those of the tibial campaniform sensilla and the tactile spine (a modified campaniform) of the cockroach, two mechanoreceptors that have been extensively studied. The femoral campaniforms on cockroach legs are involved in postural and locomotory behaviour, operating at loading frequencies below 10 Hz, where a cycle of limb movement will produce a burst of action potentials (Zill *et al.* 1981). Chapman *et al.* (1979) found that a simple linear transfer function model was sufficient to quantify the encoding properties of these campaniforms. At increased loading frequencies, however, the leg campaniform discharge becomes phase-locked and thus active over a very narrow portion of a sinusoidal stimulus. This rectification is also a feature of the campaniform neurones of the cockroach tactile spine (French and Kuster, 1981; French, 1980) and hair plate sensilla (French and Wong, 1976, 1977). The wing campaniforms described here rarely produce more than one action potential per stimulus cycle at frequencies greater than 50 Hz. Thus, in the range of frequencies encountered during flight, the behaviour of all these sensory neurones is dominated by a rectification process that limits the temporal window for spike discharge to a very narrow portion of the stimulus cycle.

The dynamic response properties of insect mechanoreceptors have been most commonly quantified using the partial differentiation model (Chapman and Smith, 1963; for reviews, see Thorson and Biederman-Thorson, 1974; French, 1988). A distinguishing characteristic of this model is that it predicts a frequency-independent phase between stimulus and response. When stimulated sinusoidally at frequencies below 10 Hz, the d-HCV neurone also displays a nearly constant phase lead (data not shown). However, at increased loading frequencies, the d-HCV neurone exhibits a monotonically decreasing phase that results from a nearly constant delay of 0.7 ms (Fig. 11). The phase contributed by a constant delay in a

dynamic system is equal to the product of the delay time and the stimulus frequency (Milsum, 1966), and consequently governs any other fixed phases in the system at high frequencies. As with the proximal wing campaniform sensilla of locusts (Elson, 1987*a*), the d-HCV must operate during flight in the frequency domain where fixed delay dominates. The cockroach femoral tactile spine sensillum exhibits a noticeable deviation from constant phase when stimulated at frequencies above 10 Hz that results from the propagation delay to the recording site (French and Kuster, 1981). However, the methods I have employed record the sensory action potentials at the site of spike initiation, and shortening the conduction path has no effect on response latency. Therefore, the constant delay unmasked at high frequencies in the d-HCV neurone must be the result of some process upstream from spike initiation. Without a detailed analysis of the membrane properties and geometry of the sensory dendrite it is difficult to speculate on the cause of the delay, but the charging time for the membrane capacitance between the sites of transduction and spike initiation is a likely candidate.

In addition to the transduction delay mentioned above, conduction delays and synaptic delays will contribute further to the net interval between the sensory stimulus and the arrival of the afferent information in the CNS. These intervals present a unique problem for mechanoreceptors, such as the wing campaniform neurones, whose relevant physiological frequency range lies within the domain where the fixed delays dominate the phase behaviour. As the fly modulates its wingbeat frequency, say from 120 to 180 Hz, the phase relationship between wing deformation and the effects of campaniform spikes in the CNS will not be maintained.

Physiological interpretation of the Wiener system model

Without an extensive intracellular analysis, it is difficult to identify the mechanical or physiological processes that account for the filtering and rectifying behaviour of the campaniform neurones. However, the results of the second-order kernel measurements of Fig. 9 suggest that the linear filter precedes rectification. If the order of the filter and rectifier in a Wiener cascade is reversed, such that $m(\cdot)$ precedes $g(t)$, then the second-order kernel is expected to be zero everywhere except on the diagonal where $t_1=t_2$ (Marmarelis and Marmarelis, 1978). The results clearly favour the filter–rectifier sequence of a Wiener cascade model. Korenberg *et al.* (1988) reached similar conclusions with the cockroach tactile spine campaniform, but included a third element, a second linear filter acting in series after the static rectifier.

The net filtering behaviour of insect mechanoreceptors might result from the dynamic properties of mechanical coupling, transduction or spike encoding. Because the point compliance of the sensilla did not vary strongly with frequency (Fig. 4), it is unlikely that the gross mechanical properties of the dome and socket play a major role in the dynamic behaviour of the neurone as a whole. Although two-thirds of the cockroach tibial campaniform sensilla examined by Chapman

et al. (1979) displayed viscoelastic behaviour, they showed that it could make only a minor contribution to the adaptation of the receptors. In *Drosophila*, the differences between the slowly and rapidly adapting campaniforms on the wing persist when the cells are stimulated with electrical pulses which completely bypass mechanical coupling (Dickinson and Palka, 1987). Thus, it is also unlikely that mechanical properties of the attachments between the dome and the sensory dendrite contribute strongly to the response dynamics. Therefore, the processes responsible for the filtering behaviour of the neurone must reside in the downstream membrane properties associated with transduction or encoding.

Although there is agreement that rectification is resident primarily in the encoding process, the relative contributions of transduction and encoding to the dynamic behaviour of insect mechanoreceptors are unclear. Mann and Chapman (1975) found that the transcuticular manifestation of the transduction current followed sinusoidal stimuli linearly, for small displacements, while the spike output remained restricted to a discrete portion of the stimulus cycle, indicating that the rectification reflects the behaviour of the spike-encoding process. By examining the dynamic behaviour of both the transduction current and the spike trains, they also concluded that both transduction and encoding contributed to the rate sensitivity. French (1984), using extracellular electrodes to study the transduction current in the cockroach tactile spine, provided strong evidence that encoding, and not transduction, was responsible for the dynamic behaviour of the neurone. However, because the transduction current was obscured by the presence of action potentials, these experiments required the use of sub-threshold stimuli. If there are spatial nonlinearities inherent to the transduction process, the frequency response to suprathreshold stimuli might be more sharply filtered. In addition, it is possible that the filtering properties of the transduction process become limiting at loading frequencies higher than the 1–100 Hz range used to stimulate the tactile spine. Thus, the relative roles of transduction and encoding in the dynamic behaviour of the d-HCV neurones, particularly at stimulus frequencies above 50 Hz, remain conjectural.

Whatever the actual physiological processes responsible for the encoding properties, it is useful to consider the two elements of the Wiener cascade model, $g(t)$ and $m(\cdot)$, in a proposed role of the campaniform sensory neurones as 'one-shot' detectors. In a Wiener system, the phase relationships between stimulus and response are set entirely by the characteristics of the linear filter $g(t)$. The subsequent rectification cannot shift the peak response, yet it acts to narrow the temporal window of spike probability. This sharpening of the neurone's response is crucial if the CNS requires an accurate measure of the timing of deformations on the wing.

Appendix

Systems analysis

The kernels of a Wiener series may be estimated using the Lee–Schetzen cross-

correlation technique (Schetzen, 1980), in which the nth-order kernels are calculated from nth-order cross-correlations of a stimulus input with the response. Using this method, the first-order kernel has the discrete form:

$$h_1(\tau) = (1/PT) \sum_{i=1}^{N} y(i\delta t)\, x\,(i\delta t - \tau)\delta t\,, \tag{A1}$$

where T is the record length, x and y are the input and output functions, respectively, τ is the time variable, and δt is the sampling period. Because the stimulus is band-limited, the power level of the input, P, is computed from the area under the autocorrelation function of the stimulus, and thus has units of $(\text{input})^2 \times \text{time}$. This method simplifies if the spike train of the sensory neurone is considered to be a string of discrete impulse functions (Bryant and Segundo, 1976; Marmarelis and Marmarelis, 1978). Let:

$$h_1(\tau) = (1/PT) \sum_{n=1}^{N} \sum_{k=1}^{K} \epsilon(n\delta t - t_k)x(n\delta t - \tau)\delta t\,, \tag{A2}$$

for which

$$\left\{ \begin{array}{l} \epsilon(t)=C_S,\ t=0 \\ \epsilon(t)=0,\ t\neq 0 \end{array} \right\}$$

where K is the total number of spikes, which occur at times t_k (k=1,2,3,... K), and C_S is a scaling coefficient equal to (1/sampling rate) (in spikes s^{-1}).

In these experiments δt, the sampling interval, is 200 μs, and thus C_S is 5000 spikes s^{-1}. Equation A2 shows that $h_1(\tau)$ is equal to 0 unless $n\delta t$ is equal to t_k, which happens whenever a spike occurs. Therefore, the expression reduces to:

$$h_1(\tau) = C_S/PT \sum_{k=1}^{K} x(t_k - \tau)\delta t \tag{A3}$$

or

$$h_1(\tau) = (C_S K/PT)x_i(\tau)\delta t\,, \tag{A4}$$

where $x_i(t)$ is the mean input preceding the occurrence, at times t_k, of each spike. The length of this 'pre-spike signal average' function is set by the system memory of the neurone, operationally defined as the time required for the pre-spike average to fall to zero. In these experiments, a value of 12.8 ms was chosen for the system memory, and longer values did not improve the predictions of the model. Note that, if the stimulus is calibrated in displacement, then $h_1(\tau)$ has the units of output input^{-1} time^{-1} or spikes s^{-2} nm^{-1}. The quantity (K/T) is simply the mean firing rate F. The coefficient C_S is the inverse of δt, and therefore expression A4 simplifies still further to:

$$h_1(\tau) = (F/P)x_i(\tau) \tag{A5}$$

or

$$h_1(\tau) = \xi x_i(\tau)\,, \tag{A6}$$

where $\xi = F/P$, which is equation 4 in the Materials and methods section. The above derivation of the linear function $h_1(\tau)$ differs somewhat from that of Bryant and Segundo (1976), and contains only two terms, the pre-spike signal average, $x_i(\tau)$, and the sensitivity parameter, ξ. The $h_1(\tau)$ function may be convolved with any arbitrary stimulus waveform to construct a linear prediction of the neurone's response.

I wish to thank John Palka, Tom Daniel and Bob Pinter for their many helpful comments and suggestions with the manuscript. This work was supported by an NSF Graduate Fellowship and NSF grant BNS-8507460 to John Palka.

References

BRYANT, H. L. AND SEGUNDO, J. P. (1976). Spike initiation by transmembrane current: a white-noise analysis. *J. Physiol., Lond.* **260**, 279–314.

CHAPMAN, K. M. AND DUCKROW, R. B. (1975). Compliance and sensitivity of a mechanoreceptor of the insect integument. *J. comp. Physiol.* A **100**, 251–268.

CHAPMAN, K. M., DUCKROW, R. B. AND MORAN, D. T. (1973). Form and role of deformation in excitation of an insect mechanoreceptor. *Nature* **197**, 699–701.

CHAPMAN, K. M., MOSINGER, J. L. AND DUCKROW, R. B. (1979). The role of viscoelastic coupling in sensory adaptation in an insect mechanoreceptor. *J. comp. Physiol.* A **131**, 1–12.

CHAPMAN, K. M. AND SMITH, R. S. (1963). A linear transfer function underlying impulse frequency modulation in a cockroach mechanoreceptor. *Nature* **197**, 699–670.

COLE, E. S. AND PALKA, J. (1982). The pattern of campaniform sensilla on the wing and haltere of *Drosophila melanogaster* and several of its homeotic mutants. *J. exp. Morph.* **71**, 41–61.

DANIEL, T. L. (1987). Forward flapping flight from flexible fins. *Can. J. Zool.* **66**, 630–638.

DICKINSON, M. H. (1990). Comparison of encoding properties of campaniform sensilla on the fly wing. *J. exp. Biol.* **151**, 245–261.

DICKINSON, M. H. AND PALKA, J. (1987). Physiological properties, time of development, and central projections are correlated in the wing mechanoreceptors of *Drosophila*. *J. Neurosci.* **7**, 4201–4208.

ELLINGTON, C. P. (1984*a*). The aerodynamics of hovering insect flight. III. Kinematics. *Phil. Trans. R. Soc. Ser.* B **305**, 41–78.

ELLINGTON, C. P. (1984*b*). The aerodynamics of hovering insect flight. IV. Aerodynamic mechanisms. *Phil. Trans. R. Soc. Ser.* B **305**, 79–113.

ELSON, R. C. (1987*a*). Integration of wing proprioceptive and descending exteroceptive sensory inputs by thoracic interneurones of the locust. *J. exp. Biol.* **128**, 193–217.

ELSON, R. C. (1987*b*). Flight motor neurone reflexes driven by strain-sensitive wing mechanoreceptors in the locust. *J. comp. Physiol.* A **161**, 747–760.

ELSON, R. C. (1987*c*). Interneuronal processing of inputs from the campaniform sensilla of the locust hindwing. *J. comp. Physiol.* A **161**, 761–776.

ENNOS, A. R. (1988*a*). The importance of torsion in the design of insect wings. *J. exp. Biol.* **140**, 137–160.

ENNOS, A. R. (1988*b*). The inertial cause of wing rotation in Diptera. *J. exp. Biol.* **140**, 161–169.

ENNOS, A. R. (1989). The kinematics and aerodynamics of the free flight of some Diptera. *J. exp. Biol.* **142**, 49–85.

FRENCH, A. S. (1980). Sensory transduction in an insect mechanoreceptor, linear and nonlinear properties. *Biol. Cybernetics* **38**, 115–123.

FRENCH, A. S. (1984). Action potential adaptation in the femoral tactile spine of the cockroach, *Periplaneta americana*. *J. comp. Physiol.* **155**, 803–812.

FRENCH, A. S. (1988). Transduction mechanisms of mechanosensilla. *A. Rev. Ent.* **33**, 39–58.

FRENCH, A. S. AND KUSTER, J. E. (1981). Sensory transduction in an insect mechanoreceptor, extended bandwidth measurements and sensitivity to stimulus strength. *Biol. Cybernetics* **42**, 87–94.

FRENCH, A. S. AND WONG, R. K. S. (1976). The responses of trochanteral hair plate sensilla in the cockroach to periodic and random displacements. *Biol. Cybernetics* **22**, 33–38.

FRENCH, A. S. AND WONG, R. K. S. (1977). Nonlinear analysis of sensory transduction in an insect mechanoreceptor. *Biol. Cybernetics* **26**, 231–240.

GHYSEN, A. (1978). Sensory neurones recognize defined pathways in *Drosophila* central nervous system. *Nature* **274**, 869–872.

GNATZY, W., GRÜNERT, U. AND BENDER, M. (1987). Campaniform sensilla of *Calliphora vincina* (Insecta, Diptera). I. Topography. *Zoomorphology* **106**, 312–319.

GÖTZ, K. G. (1986). Course-control, metabolism and wing interference during ultralong tethered flight in *Drosophila melanogaster*. *J. exp. Biol.* **128**, 35–46.

HEIDE, G. (1983). Neural mechanisms of flight control in diptera. In *Biona Report 2: Insect Flight* (ed. W. Nachtigall), pp. 35–52. Stuttgart: Fischer.

HENGSTENBERG, R. (1988). Mechanosensory control of compensatory head roll during flight in the blowfly *Calliphora erythrocephala* Meig. *J. comp. Physiol.* A **163**, 151–165.

HENGSTENBERG, R., SANDEMAN, D. C. AND HENGSTENBERG, B. (1986). Compensatory head roll in the blowfly *Calliphora* during flight. *Proc. R. Soc.* B **227**, 455–482.

HORSMANN, U. AND WENDLER, G. (1985). The role of a fast wing reflex in locust flight. In *Insect Locomotion* (ed. M. Gewecke and G. Wendler), pp. 157–165. Berlin: Paul Parey.

HUNTER, I. W. AND KORENBERG, M. J. (1986). The identification of nonlinear biological systems, Wiener and Hammerstein cascade models. *Biol. Cybernetics* **55**, 135–144.

KORENBERG, M. J., FRENCH, A. S. AND VOO, S. K. L. (1988). White-noise analysis of nonlinear behaviour in an insect sensory neuron, kernel and cascade approaches. *Biol. Cybernetics* **58**, 313–320.

MANN, D. W. AND CHAPMAN, K. M. (1975). Component mechanisms of sensitivity and adaptation in an insect mechanoreceptor. *Brain Res.* **97**, 331–336.

MARMARELIS, P. Z. AND MARMARELIS, V. Z. (1978). *Analysis Of Physiological Systems, The White Noise Approach.* New York: Plenum Press.

MARMARELIS, P. Z. AND NAKA, K. (1972). White noise analysis of a neuron chain: an application of Wiener theory. *Science* **175**, 1276–1278.

MARMARELIS, V. Z. (1988). Coherence and apparent transfer function measurements for nonlinear physiological systems. *Ann. biomed. Eng.* **16**, 1–15.

MILSUM, J. H. (1966). *Biological Control System Analysis.* New York, London: McGraw Hill.

MORAN, D. T., CHAPMAN, K. M. AND ELLIS, R. A. (1971). The fine structure of cockroach campaniform sensilla. *J. Cell Biol.* **48**, 155–173.

NACHTIGALL, W. (1966). Die Kinematik der Schlagflügelbewegungen von Dipteren. Methodische und analytische Grundlagen zur Biophysik des Insektenflugs. *Z. vergl. Physiol.* **22**, 155–211.

NACHTIGALL, W. (1979). Rasche Richtungsänderungen und Torsionen schwingender Fliegenflügel und Hypothesen über zugeordnete instationäre Strömungseffekte. *J. comp. Physiol.* A **133**, 351–355.

NACHTIGALL, W. (1981). Insect flight aerodynamics. In *Locomotion and Energetics in Arthropods* (ed. C. F. Herreid and C. R. Fourtner), pp. 127–162. New York: Plenum Press.

PALKA, J., LAWRENCE, P. A. AND HART, H. S. (1979). Neural projections from homeotic tissue of *Drosophila melanogaster* studied in bithorax mutants and mosaics. *Devl Biol.* **69**, 549–575.

PALKA, J., MALONE, M. A., ELLISON, R. L. AND WIGSTON, D. J. (1986). Central projections of identified *Drosophila* sensory neurons in relation to their time of development. *J. Neurosci.* **6**, 1822–1830.

SCHETZEN, M. (1980). *The Volterra and Wiener Theories of Nonlinear Systems.* New York: John Wiley & Sons.

SOKAL, R. R. AND ROHLF, F. J. (1981). *Biometry.* San Francisco: W. H. Freeman.

SPINOLA, S. M. AND CHAPMAN, K. M. (1975). Proprioceptive indentation of the campaniform sensilla of cockroach legs. *J. comp. Physiol.* **96**, 257–272.

THORSON, J. AND BIEDERMAN-THORSON, M. (1974). Distributed relaxation processes in sensory adaptation. *Science* **183**, 161–172.

VOGEL, S. (1967). Flight in *Drosophila*. III. Aerodynamic characteristics of fly wings and wing models. *J. exp. Biol.* **46**, 431–443.

WEIS-FOGH, T. (1973). Quick estimates of flight fitness in hovering animals, including novel mechanisms for lift production. *J. exp. Biol.* **59**, 169–230.

WOOTON, R. J. (1981). Support and deformability of insect wings. *J. Zool., Lond.* **193**, 447–468.

ZACWILICHOWSKI, J. (1931). Über die Innervierung und die Sinnesorgane der Flügel der Insekten. *Bull. Acad. pol. Cl. Math. Nat.* **I, II**, 391–424.

ZILL, S. N., MORAN, D. T. AND VARELA, F. G. (1981). The exoskeleton and insect proprioception. III. Activity of tibial campaniform sensilla during walking in the american cockroach, *Periplaneta americana*. *J. exp. Biol.* **94**, 57–75.